JOURNAL OF GEOPHYSICAL RESEARCH, VOL. 113, E06001, doi:10.1029/2007JE002916, 2008

Low-energy electron current in the Martian tail due to reconnection of draped interplanetary magnetic field and crustal magnetic fields

Demet Uluşen[1] and Ivan Linscott[1]

Received 15 March 2007; revised 11 October 2007; accepted 6 March 2008; published 12 June 2008.

[1] We observe seasonal, nighttime clustering of significant enhancements in the Mars Global Surveyor electron omnidirectional flux data at low-energy levels over a specific geographical region at the west edge of the crustal fields (at around 70°S and between 30°E and 150°E). We propose that photoelectrons generated over the crustal sources on the Martian dayside are transported along lines of the reconnected interplanetary magnetic field to the nightside and populate currents formed in the magnetotail. Comparison of the draping direction (estimated from the dayside data between 50° and 60°N latitude band over the northern hemisphere) at the closest time of the enhancements with the crustal fields at ~150°E and ~65°S shows the existence of favorable conditions for the reconnection. Seasonal variation observed in the draping direction accounts for the seasonal nature of the phenomenon. Moreover, a nearly 25 d periodic variation of the draping direction, due to solar rotation, strictly coincides with the periodic variation observed in the strength of the enhancements. We also demonstrate the effect of the Sun on the electron flux variations over two regions: (1) closed crustal fields and (2) the enhancement clustering region. Finally, we propose a model for the distribution of current sources on the nightside that accounts for the perturbations observed in the magnetic field data.

Citation: Uluşen, D., and I. R. Linscott (2008), Low-energy electron current in the Martian tail due to reconnection of draped interplanetary magnetic field and crustal magnetic fields, *J. Geophys. Res.*, *113*, E06001, doi:10.1029/2007JE002916.

1. Introduction

[2] Mars has no global internal magnetic field. Thus the solar wind is expected to interact directly with the Martian ionosphere and upper atmosphere [*Nagy et al.*, 2004]. However, *Acuña et al.* [1998] discovered that Mars has strong local crustal magnetic sources located mostly around the midlatitudes in the southern hemisphere whose magnitudes can exceed 200 nT at an altitude of 400 km. As Mars rotates on its axis, the strong crustal fields presents both a temporally and spatially variable obstacle to the solar wind [*Acuña et al.*, 1999; *Connerney et al.*, 1999; *Purucker et al.*, 2000; *Ness et al.*, 2000; *Crider*, 2004]. The effect of the crustal fields is much more pronounced at low altitudes near the anomalies.

[3] Mars does not have a constant, stable, and permanent region of confined radiation like the Earth's radiation belts, but the discovery of the strong crustal magnetic sources raised the possibility that local regions of magnetic confinement might exist over the crustal sources. Initial investigations of the nature of these crustal sources revealed that the closed field regions facing sunlight are filled with photoelectrons [*Mitchell et al.*, 2001]. When these same regions rotate into shadow, the photoelectrons disappear due to recombination and absorption, forming plasma voids comparable in size to the closed field regions. These voids are effectively cut off from solar wind plasma that is traveling up to the magnetotail and from the sunlit hemisphere [*Mitchell et al.*, 2001]. The same regions may experience other transient events, especially electron density enhancements, due to the interaction of these regions with the solar wind [*Soobiah et al.*, 2006; *Krymskii et al.*, 2002]. For example, *Brain et al.* [2006a] correlated auroral emissions with the electron flux enhancements in the vicinity of the crustal sources at energy levels between 100 eV and 2.5 keV suggesting the reconnection of crustal magnetic fields with the draped interplanetary magnetic field (IMF) and subsequent precipitation of sheath particles at lower altitudes [*Ness at al.*, 2000; *Mitchell et al.*, 2001; *Krymskii et al.*, 2002; *Brain et al.*, 2003]. Furthermore, recent studies of *Ferguson et al.* [2005] and *Halekas et al.* [2006] showed that current sheets are formed in the tail extending to low altitudes (~400 km) and induce magnetic fields in their neighborhood. *Dubinin et al.* [2006a] reported permanent localized strip-like structure of plasma densities on a number of Mars Express (MEX) orbits, where the structures were aligned tailward of the terminator plane and composed of magnetosheath-like electrons and planetary ions. These structures can be important in the plasma inflow to the

[1]Department of Electrical Engineering, Stanford University, Stanford, California, USA.

0148-0227/08/2007JE002916$09.00

magnetosphere and planetary plasma transport to the tail [*Dubinin et al.*, 2006a, 2006c]. Similarly, *Frahm et al.* [2006a] reported photoelectron peaks recorded by the MEX Electron Spectrometer (ELS), implying electron flows away from Mars near the terminator and in the tail, which are probably produced on the dayside and carried to the tail by the field lines [*Frahm et al.*, 2006b; *Fedorov et al.*, 2006].

[4] In this paper, we discuss a transient phenomenon we have observed near the crustal sources, likely due to reconnection of the crustal fields and draped IMF lines, yet different in nature from the auroral events. We observe a distinct region at the west edge of the crustal sources in the southern hemisphere having anomalously intense low-energy electrons with spectra that differ from those in the regions where typical auroras are found. We propose and articulate a mechanism for these events involving the reconnection of the draped IMF with crustal fields on the dayside that stretches to the nightside carrying and accelerating photoelectrons toward the tail producing a current consisting of locally generated electrons that flows from the dayside to the nightside. Similar to our observations, the intensifications in the low-energy electron fluxes and the possibility of their originating on the dayside were noted by *Halekas et al.* [2006].

[5] This paper consists of five sections. In section 2, we give a detailed description of geometry and the Mars Global Surveyor (MGS) data used in our observations. In section 3, we illustrate our observations of the phenomenon and its seasonal nature. In section 4, we discuss alternative source mechanisms of the phenomenon and consider the key physical properties and requirements for reconnection of the draped IMF with crustal fields. We also discuss the periodicity of the phenomenon and its correlation with the periodicity seen in the draped IMF. Taking into account the precession of Mars' rotation axis during one Martian year additionally allows us to confirm the expected variations in the electron flux over two distinctive local regions. Finally, in section 5, we focus on the magnetic field perturbations in the vicinity of the enhancements and demonstrate models of the current sources that are responsible for these perturbations.

2. Geometry and MGS Data

[6] The mapping phase of MGS began in March 1999 and ended in November 2006. In this study, over 6 years worth of magnetometer and electron reflectometer (MAG/ER) data were used, acquired during the mapping phase between March 1999 and May 2005 and released by the Goddard Space Flight Center of NASA to the Planetary Data System (PDS) at the University of California, Los Angeles (UCLA). During this period, the polar orbit of MGS was nearly circular at an altitude of 400 km, fixed at 0200–1400 LT, with MGS completing an orbit every 2 h and orbiting almost 12 times in one Martian day.

[7] The MGS MAG/ER instrument consists of two redundant triaxial fluxgate magnetometers (MAG) and an electron reflectometer (ER). The MAG produces magnetic field vector measurements up to 32 samples per second over the range from ±4 nT to ±65,536 nT while the ER measures the local electron flux (in cm^{-2} s^{-1} sr^{-1} eV^{-1}) averaged over a $360^\circ \times 4^\circ$ disk-shaped field of view in 19 different energy channels between 10 eV and 20 keV every 2 s, with an energy resolution of 25%. This energy range allows for observation of ionospheric, sheath, and solar wind plasma. Detailed description of the MGS MAG/ER instrument and data processing is given by *Acuña et al.* [1992, 2001].

[8] In order to remove redundancy and to reduce the size of 6 years worth of data, the vector measurements of magnetic field and omnidirectional electron flux data were first averaged to have a spatial resolution of a 1° by 1° grid over a spherical surface at 400 km altitude. This reduction was achieved by averaging the samples that fell into the same grid point along a track using position information in MAG data files and time information in ER data files. This way the average sampling duration for both magnetic field and electron flux data was standardized to 10 s. Because of compression and expansion of the grid points in longitude at the poles and at the equator, respectively, the along-track samples are almost 2 s near the poles and 21 s near the equator. These averages were sorted or binned into individual data sets labeled by factors that influence the plasma environment such as season and time of day.

3. Observation of the Significant Enhancements in the Low-Energy Electron Flux and Characteristic Spectra

[9] In examining the data sets produced by the above method, we found significant enhancements in the low-energy electron fluxes at the west edge of the crustal sources during nighttime. In the ER data, low-energy omnidirectional electron fluxes (below approximately few hundred eV) exhibit sharp enhancements of ~2 orders of magnitude as MGS proceeds north to south at around 70°S on the nightside of the planet. An example of these enhancements is shown in Figure 1a, and the deviations in the magnetic field components during this event are shown in Figure 1b. The curves in Figure 1a present omnidirectional electron fluxes at 19 different energy levels between 11 eV and 16 keV on a logarithmic scale. (Only six energy levels are labeled in red on the plot for clarity.) Here the lowest energy electrons have highest flux values. Electrons with energies below a few hundred eV exhibit the behavior we define as significant enhancements. The discontinuities seen in some of the energy levels are due to saturation of the ER instrument. The curves in Figure 1b show the three components of the magnetic field simultaneous to the ER flux records in the Sun-state coordinate system (SS) (which is the same as Mars solar orbital the (MSO) coordinate system: the x axis points at the Sun, the y axis is antiparallel to Mars' orbital velocity, and the z axis completes the right-handed system). The average time interval that MGS spends in these enhancements is about 200 s, during which it moves about 650 km along its orbit.

[10] To characterize this phenomenon, we mapped the percentage of occurrences of the significant enhancements among all nightside southern hemisphere observations during the 6 years period for each of the 19 energy levels in Figure 1. The energy band over which significant enhancements are detected covers the range from 10 eV to a few hundred eV. The percentage occurrence maps distinguish the enhancements by selecting the observations having 2 orders of magnitude more electron flux than the ambient

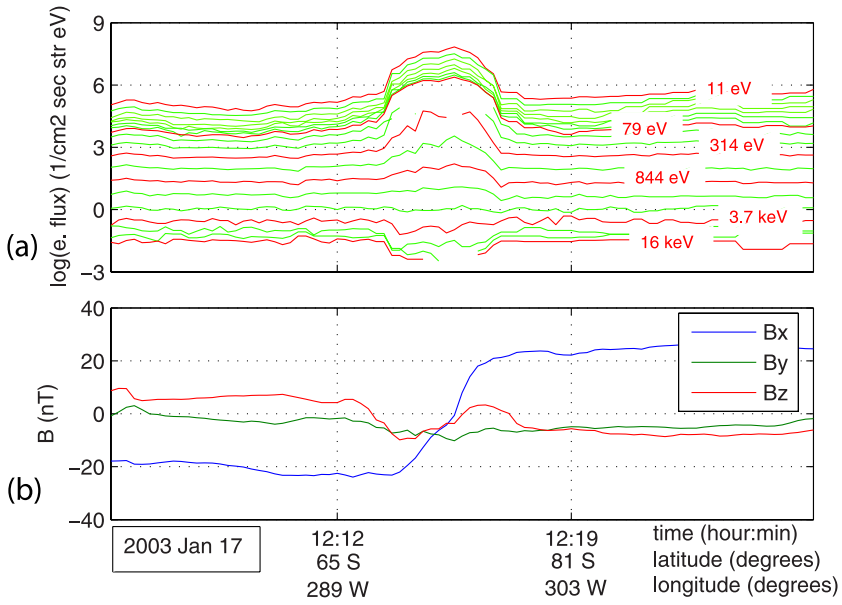

Figure 1. An example of a significant enhancement observed over the region between 30° and 120°E and at ~70°S. The x axis presents the time evolution as MGS moves from north to south on the nightside over the region of interest. (a) The logarithm of the omnidirectional electron fluxes at 19 energy levels, six of which are indicated on the curves, (the energy levels from top (10 eV) to bottom (20 keV) with energy resolution of 25%). (b) The magnetic field components in the Sun-state coordinate system at the time MGS records the significant enhancement.

levels at energies below ~200 eV. Figure 2 shows one such percentage map for the 61 eV energy band. One evident feature in these maps, and displayed in Figure 2, is that at low-energy levels the significant enhancements appear to cluster in a local geographical area, between 30° and 120°E, and at around 70°S. As can be inferred from the map, there are other locations scattered over the southern hemisphere where enhancements are observed at a lower rate. (This is also the case for the northern hemisphere.) However, typical properties of the enhanced energy distributions in the cluster (discussed in sections 4 and 5) cannot be statistically determined in the scattered regions due to the low observation rate. Thus, in this study, our focus is on the cluster seen on the bottom left corner of the map (between 30° and 120°E, and at around 70°S).

[11] The cluster's enhanced low-energy distribution suggests that the electrons in this region may have spectral characteristics that differ from those found in typical nightside spectra. Figure 3 shows that for a representative point in the cluster those electrons have a spectrum that is strongly enhanced at low energies (solid line). This representative spectrum is obtained by averaging over the cluster region spectra from places where the significant enhancements have been identified. While passing through the region with the enhancements, the ER instrument almost always saturates for electron energies above 79 eV (see Figure 1). The saturated measurements are not included in the averaging process. The averaging reveals a kink near 100 eV implying higher electron fluxes in the vicinity of the kink. (Clustering of low-energy electrons over the same region was noted by *Halekas et al.* [2006].) The phenomenon we observe is different from the auroral events observed by *Brain et al.* [2006a], which are mostly seen around the crustal fields and at higher energy levels. For comparison, a representative spectrum of auroral events is illustrated with the representative spectrum of the significant enhancements in Figure 3. The averaged spectrum of the auroral events (starred line) was obtained from the measurements having peaked electron spectra between 100 eV and 2.5 keV over the region centered near 150°E, 70°S, where most auroral events are accumulated [*Brain et al.*, 2006a]. As seen in Figure 3, the spectra are very different below a few hundred eV. We also compare the

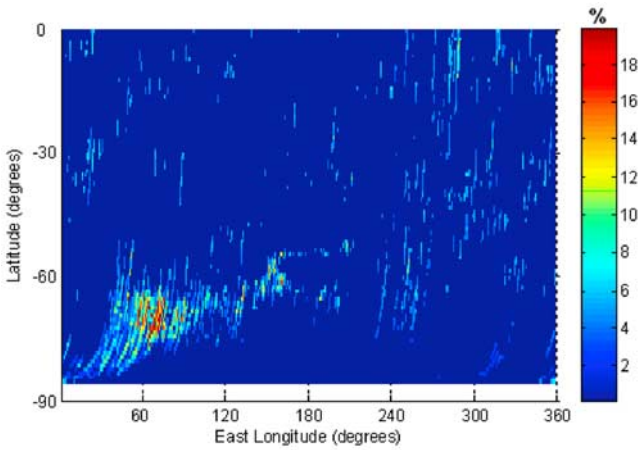

Figure 2. The map of the percentage of the significant enhancements at 61 eV energy band among all nightside observations over the southern hemisphere. This map represents the general characteristics of all low energies below a few hundred eV.

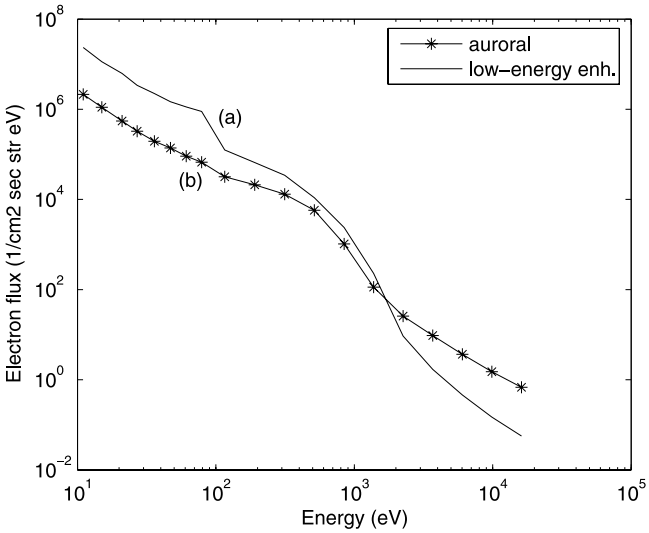

Figure 3. Comparison of electron energy spectra of two different regions, which is obtained using the MGS ER data. Curve a, the solid line, presents the averaged spectrum of the significant enhancements observed between 30° and 120°E and at ~70°S. Curve b, the starred line, presents the averaged spectrum of aurorae observed at around 150°E, 70°S.

electron energy distribution of the enhancements and of the plasma recorded in the permanent localized strip-like structures along the wake boundary reported by *Dubinin et al.* [2006a]. The energy spectrum obtained using MEX electron flux measurements in these strip-like structures peak at ~80 eV, which is the typical energy of the magnetosheath electrons, and is not enhanced at low-energy levels, unlike the spectrum observed in the significant enhancements. Although the spectrum of these strip-like structures implies a magnetic connection of the IMF with the crustal field lines, *Dubinin et al.* [2006a] found no evident correlation between the positions of the crustal sources and these localized strip-like structures.

[12] Temporal distribution of the patch-like clustering exhibits periodicities on both a ~25 day timescale and a seasonal timescale. The seasonal variation is illustrated in Figure 4 by presenting the variation of the occurrence of the enhancements with respect to the areocentric longitude of the Sun, Ls. (i.e., the Martian northern hemisphere seasons). Conditions for the significant enhancements are more favorable in the Martian northern hemisphere spring and summer.

4. Proposed Source of the Localized Significant Enhancements and Their Periodic Nature

[13] In this section, we will discuss the possible source region and source mechanism of the significant enhancements. The fact that the enhancements are observed on the nightside and the magnetic field reversals occur at the location of the enhancements suggests that the phenomenon may be due to the transport of the ionospheric electrons by the draped IMF, which drags them through the ionosphere and slips around the poles and sides of Mars. Then electrons may be accelerated by the field aligned electric fields and pushed toward the central tail under the influence of the magnetic field tension forces $\mathbf{J} \times \mathbf{B}$. (This process is also one of the probable mechanisms responsible for the formation of the plasma and current sheets observed in the tail [*Halekas et al.*, 2006; *Frahm et al.*, 2006b; *Dubinin et al.*, 2006b].) However, this by itself cannot be adequate because, if it were, the enhancements would be observed over the entire nightside hemisphere of Mars rather than just clustering in a localized region in the southern hemisphere. Moreover, they would occur anytime during the entire Martian year rather than only in the northern hemisphere late in spring and early summer.

[14] Considering the local clustering of the enhancements, an alternative scenario would be to stretch the closed field lines formed over the crustal sources on the dayside from the formation region around the dawnside of Mars toward the magnetotail. In that case, electrons already trapped in the closed fields would follow the field lines, remaining trapped by moving in both directions along these lines. However, this mechanism is in contradiction to the magnetic field data in the vicinity of the enhancements, which imply a current dominant in one direction (in the (+) azimuthal direction). The existence of a regular temporal structure in the occurrence of the enhancements and simultaneous magnetic field perturbations make other possible

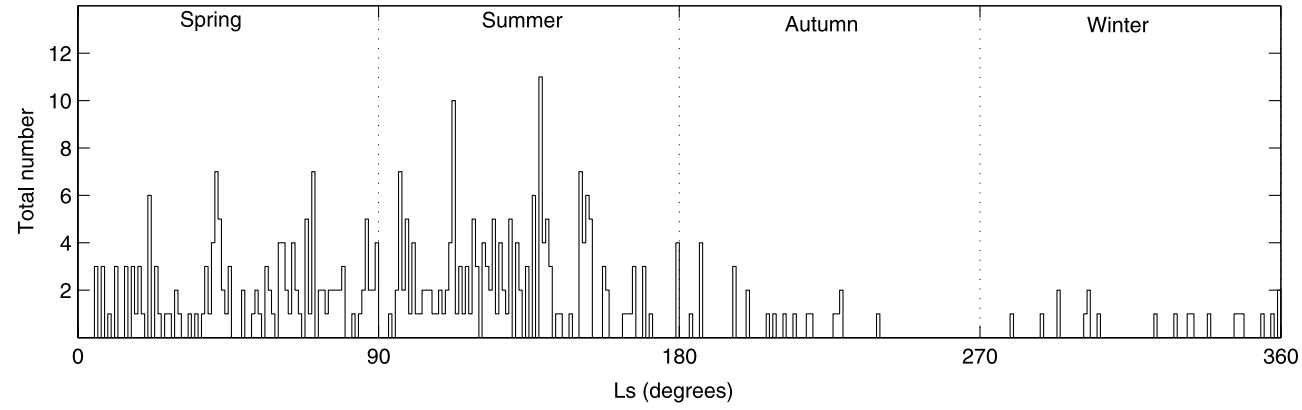

Figure 4. Variability of the occurrence of the enhancements with respect to areocentric longitude of the Sun (Ls). The Martian seasons are indicated on the top.

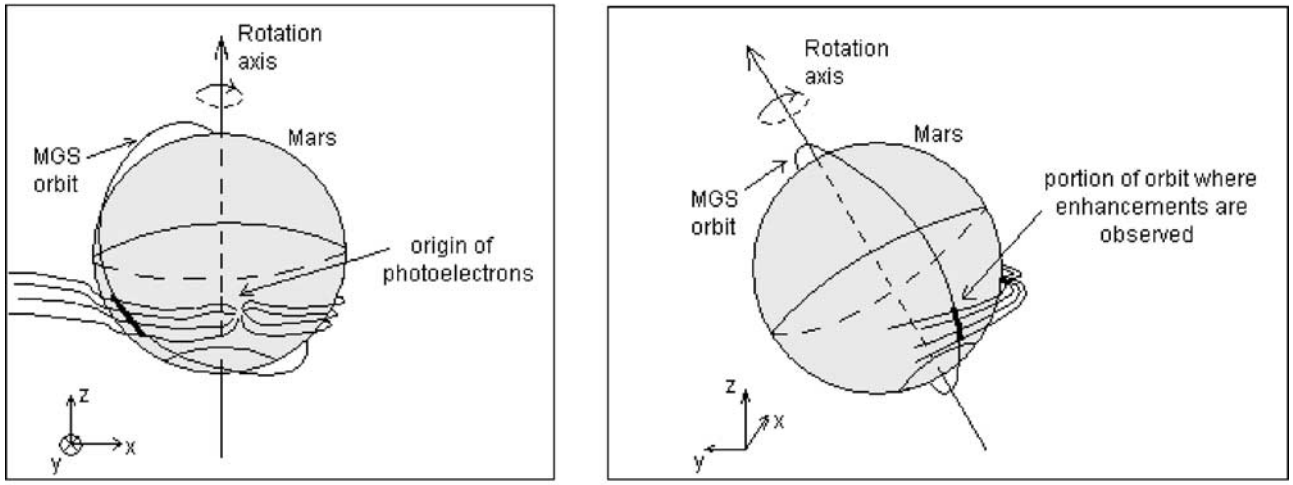

Figure 5. Relative positions of Mars, the MGS orbit, the crustal sources, and the draped field lines in the SS coordinate system at the time an enhancement is observed. (left) The side view. (right) The view from an angle on the nightside. Reconnected and draped IMF lines carry the photoelectrons from the dayside to the nightside, and a current form in the tail. The MGS orbit traverses the current obliquely on the nightside. The marked region shows the portion of the MGS orbit over which the enhancement is observed and the magnetic reversals are recorded in the middle of this marked region.

sources (such as the presence of a minimal nightside ionosphere, ionospheric irregularities or ionospheric clouds originating from the dayside) unlikely as the formation mechanism for this phenomenon.

[15] Considering the local clustering, the temporal distribution, and the low-energy nature of the enhancements we propose the following mechanism as the source of the observed enhancements: The photoelectrons generated over the crustal sources on the Martian dayside are transported along reconnected IMF lines to the nightside and populate the currents formed in the tail. During this process, solar wind electrons have access to the lower magnetospheric or upper ionospheric regions and may also be carried by the reconnected field lines, forming a mixture of sheath and planetary plasma. In Figure 5, the relative positions of Mars, reconnected field lines, the MGS orbit, and the location of the enhancement are illustrated from two points of view in the SS coordinate system. As can be inferred from Figure 5, at the time of the enhancements, the MGS orbit crosses the reconnected and draped field lines, in which the low-energy photoelectrons are flowing from the dayside to the nightside. The field reversals seen in Figure 1, occur in the middle of the marked region on the MGS orbit over, which enhancements are observed. Given this interpretation, the phenomenon is most likely to occur when the draped IMF direction and the field line orientation of the crustal sources are aligned for reconnection, and the magnitudes of the fields are comparable at the reconnection site. Moreover, the source region of the low-energy electrons should be exposed to the Sun at the time the enhancements are recorded. During this process, field aligned electric fields and magnetic tension forces may accelerate the electrons to higher energy levels and movement of the electrons toward central tail may be due to draping of the field lines.

[16] Our proposed scenario implies that the signatures of ionospheric photoelectrons should be present in the spectra recorded during the enhancements. Two major photoelectron peaks at $\sim$20 eV and $\sim$30 eV are produced in the CO_2 dominated atmosphere of Mars, which are due to ionization of O and CO_2 [*Frahm et al.*, 2006a]. However, the energy resolution of the ER instrument (25%) is too coarse to resolve the photoelectron peaks, and they unfortunately cannot be distinguished in the data (e.g., Figure 3). Dispersion at low energies due to further particle interactions during the photoelectrons' travel from the dayside to the nightside may also contribute to loss of the peaks in the observed spectra. Furthermore, assuming the acceleration mechanism for aurora is operating most of the time during the enhancements, the smoothed peak between 100 eV and 2.5 keV implies the presence of sheath plasma along with the planetary plasma during these events. In addition to our own analysis, we investigated an energy spectrum such as presented in Figure 3, in the work by *Soobiah et al.* [2006], where the electron energy distribution recorded by MEX/ELS during its pass over a cusp region on the dayside has a similar signature. The Soobiah spectrum is a smoothed and degraded version of the spectrum detected during enhancements, due perhaps to particle interactions and heating as the plasma evolves from day to night.

[17] The most probable source of electrons is located at the west edge of the magnetic crustal sources at 65°S, 150°E. This location is closest to the enhancements and most active in terms of auroral events. (Most of the auroral events are observed over the region centered at 70°S, 150°E [*Brain et al.*, 2006a].) In the work by *Connerney et al.* [2001], these sources are oriented eastward (radially outward field at the west of 150°E and radially inward field at the east of 150°E along 65°S). Reconnection of the crustal field lines with the draped IMF would be easiest if the IMF were oriented westward. To see if this is indeed the case, we estimated the direction of the draped IMF at 400 km. *Brain et al.* [2006b] first proposed a method of using magnetic field data recorded on the dayside over the northern hemisphere (where crustal fields are absent in the latitude band

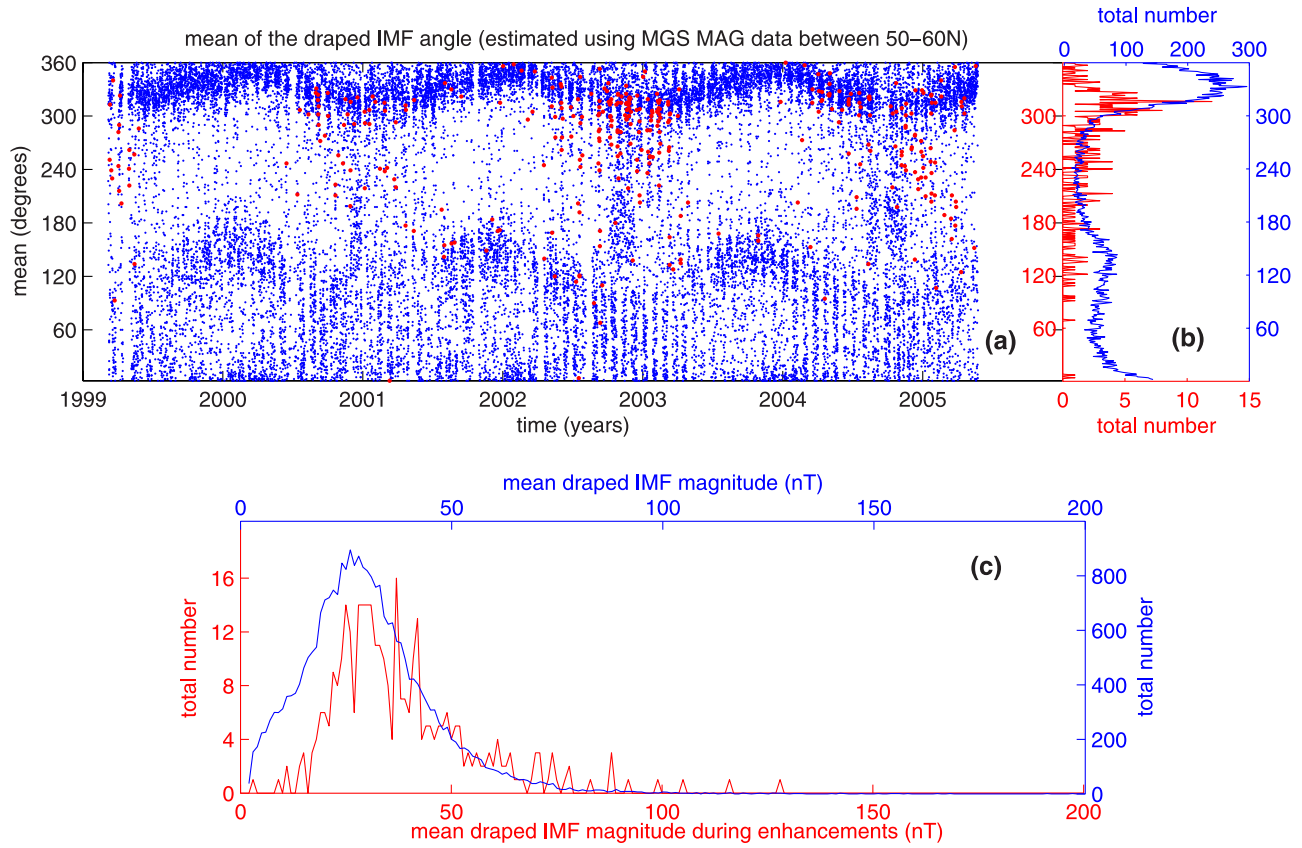

Figure 6. The direction and magnitude of the draped IMF obtained from the MGS MAG data between 50° and 60°N. (a) Mean of the draped IMF angle at each pass during 6 year time period. The red dots mark the passes on which the significant enhancements are observed over the region of interest. (b) Histogram of the mean angles obtained from all observations in 6 year time period (blue curve) and the histogram of the mean angles obtained from the observations at the times of the enhancements (red curve). (c) Histogram of the mean magnitude of the draped IMF obtained from all observations in 6 year time period (blue curve) and the histogram of the mean draped IMF magnitude obtained from the observations at the times of enhancements (red curve).

between 50° and 60°N) as a rough estimate of the draped IMF direction. Using this method, we obtained the angle between the phi and theta components (in a body-centered spherical coordinate system) of the local magnetic field and use it as the approximate direction of the draped IMF. (The horizontal component of the draped field reaches 100 nT while the magnitude of the radial components is below 4(±2) nT 75% of the time.) Thus an estimate of the direction of the draped IMF is the angle

$$\mathrm{IMF}_{\mathrm{angle}} = \arctan\left(\frac{Bp}{Bt}\right) \quad (1)$$

Note that when the draped IMF is fully southward, this angle is 0°, and when the draped IMF is fully eastward, this angle is 90°.

[18] Figure 6a shows the mean of the direction of the draped IMF estimated via equation (1) at each pass, over 6 years, determined over the latitude band (50°–60°N) in the northern hemisphere. The time period between each pass of MGS is about 2 h, which adds up to ~27,000 passes in the time period of interest. Furthermore, at each pass there are many measurements (10 samples on average) in this latitude band. The mean angle for each pass is obtained by summing the unit direction vectors of these magnetic field measurements. In this averaging we eliminated erroneous outliers, which are defined to be the ones that lie outside of the ±90° band centered at the mean. Following this approach, the standard deviation of the mean angle is less than 60°, 80% of the time. It should be noted that the IMF direction changes on many timescales and thus an estimate obtained from a small portion of the orbit does not necessarily represent the orientation throughout the entire orbit. However, for our purpose, the IMF was assumed to be constant over an orbit and represented by the estimate obtained from the 50°–60°N latitude band. Figure 6a displays the periodicity in the mean angle on the almost 2 Earth year timescale corresponding to one Martian year. This variation is caused by the change of the orientation of the rotation axis of Mars with respect to the Sun. If we zoom in to a time in CY 2003 in Figure 6a (Figure 10b, top), another periodicity, on a ~25 day timescale, becomes evident. This is associated with the solar rotation period [*Brain et al.*, 2006b].

[19] In the IMF mean angle versus time plot in Figure 6a, the red dots mark the passes on which we observed

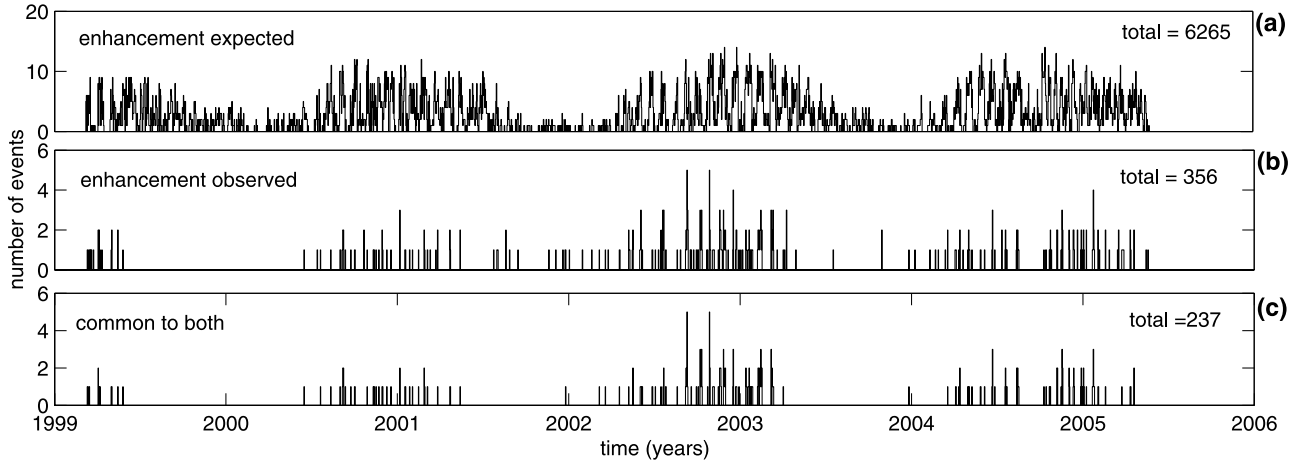

Figure 7. Variability of the occurrence of the reconnection conditions and the enhancements with respect to time (years). (a) Histogram of the passes when the reconnection conditions were met and the significant enhancements were expected. (b) Histogram of the passes when the significant enhancements were observed. (c) Common points of Figures 7a and 7b indicating the passes on which reconnection was expected and an enhancement was observed.

significant enhancements over the region of interest. Their total number is 356 out of ~27,000. Figure 6b presents the histogram of the mean angles obtained by the projection of the data on the right-hand side of the plot in Figure 6a. The blue curve in Figure 6b shows the histogram produced by using all observations over a 6 year time period while the red curve shows the histogram obtained from the observations at times of enhancements. This plot reveals that the draped IMF angle lies mostly between 230° and 330° (thus oriented westward) during the enhancements. The opposite alignment of the estimated IMF direction with respect to the potential crustal sources centered at around 150°E, 65°S favors their reconnection at the times of these events. Similarly we found that the magnitude of the draped IMF is between 20 and 60 nT at the times of enhancements. This is shown on the histograms plotted in Figure 6c.

[20] A mechanism that accounts for the seasonal nature of the occurrence of the enhancements (Figure 4) is the seasonal variation of the draped IMF direction. The six histograms presented in Figures 7 and 8 illustrate the relationship between the draped IMF direction and the seasons. They were constructed by identifying passes that met our detection criteria (see below) among all data in an approximately 6 year time period, which is about 27,000 records in total. Figures 7a–7c are histograms with respect to time while Figures 8a–8c are with respect to areocentric longitude of the Sun (Ls, i.e., the Martian northern hemisphere seasons). Figure 7a shows the number of the MGS

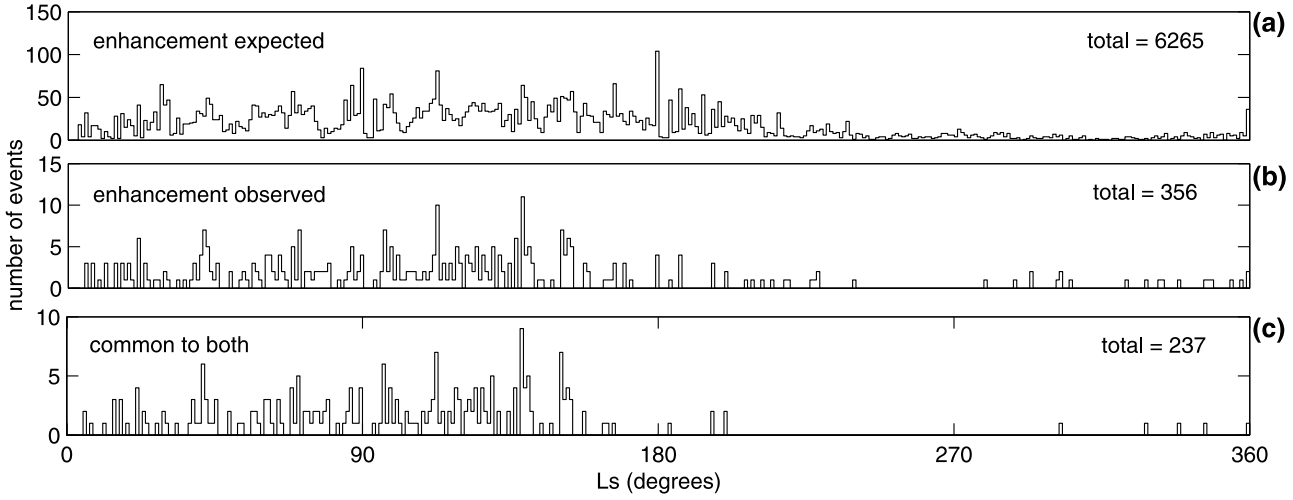

Figure 8. Variability of the occurrence of the reconnection conditions and the enhancements with respect to Martian seasons (Ls). (a) Histogram of the passes when the reconnection conditions were met and the significant enhancements were expected. (b) Histogram of the passes when the significant enhancements were observed. (c) Common points of Figures 8a and 8b indicating the passes on which reconnection was expected and an enhancement was observed.

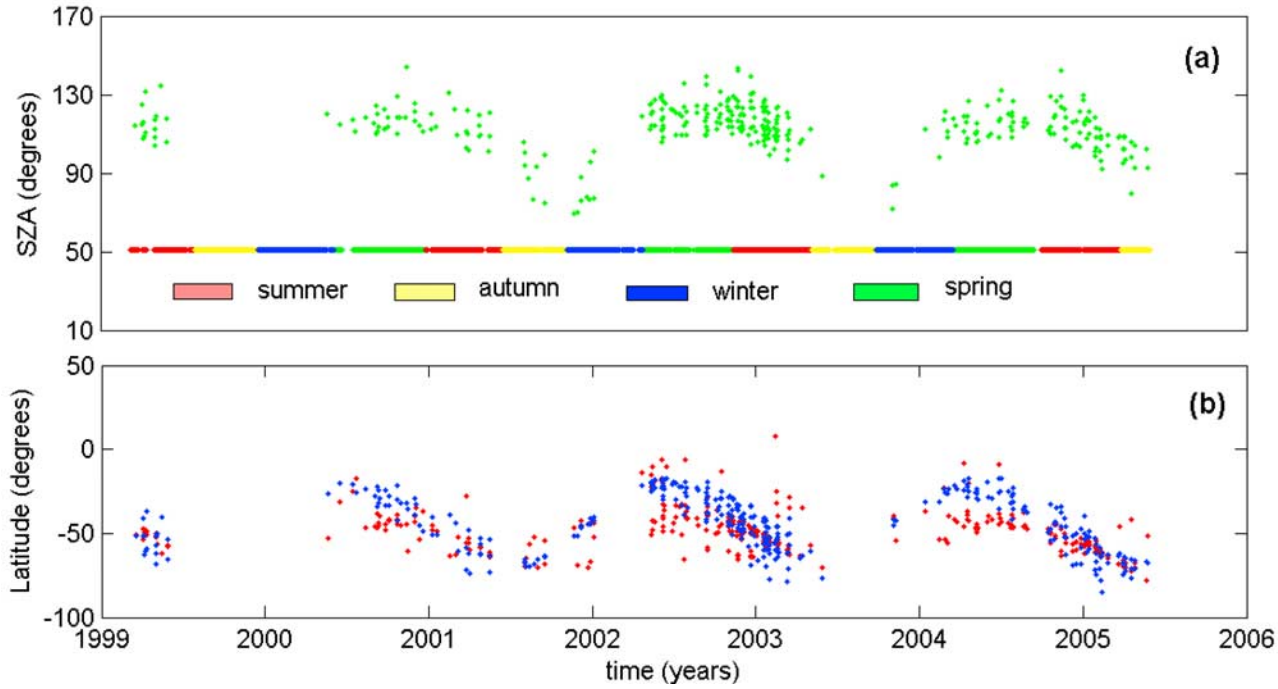

Figure 9. (a) The solar zenith angles of the crustal source region at the times of enhancements. (b) The temporal distribution of the midlatitudes of the enhancements (red dots) and of the latitudes of the source region (blue dots) at the times of the enhancements, in the SS coordinate system.

passes when the conditions for reconnection held (westward oriented IMF, i.e., 230° < IMF_{angle} < 330°). The total number of these passes is ∼6200. Note the seasonal periodicity in the distribution. Figure 7b shows the number of passes with respect to time in which we clearly observed enhancements, in a total of 356 passes. Finally, Figure 7c shows the common points of Figures 7a and 7b, which is 237 passes in total. Nearly 70% of the time, when the expected conditions for reconnection are met, the enhancements are observed. Figures 8a–8c illustrate the distribution of the number of the passes with respect to Ls rather than time, with the same criteria used in Figure 7. Thus Figure 8a shows the number of the MGS passes in which the conditions for reconnection were met, where we infer the westward alignment of the draped IMF occur most frequently in the late spring and early summer and least frequently in the late autumn and early winter. Figure 8b shows the number of passes in which we clearly observed enhancements, and Figure 8c shows the common points of Figures 8a and 8b with respect to Ls, indicating clear preference of the enhancements for the first half of the year.

[21] In addition to being the region closest to enhancements and the most active in terms of auroral events, the location of the crustal field sources (at ∼150°E, ∼65°S) is attractive, as it supports our proposal illustrated in Figure 5. Accordingly, these sources need to be illuminated by the Sun when the enhancements occur on the nightside. The highest solar zenith angles (SZAs) at which the upper ionosphere and exobase are illuminated are 120° and 110°, respectively, thus requiring that the SZAs of the proposed crustal sources must lie below these values at the times the enhancements are observed. Figure 9a illustrates the temporal distribution of the solar zenith angle of this source region at the time of the enhancements. As shown, most of the time, the SZA of the sources lies below 120°. Furthermore, the eastward foot of the closed field lines should have even lower SZAs considering the relative position of the eastward foot with respect to the center of the source during the northern late spring and early summer (the time period in which the enhancements are observed). This means that the requirement stated above is satisfied most of the time. Requiring that the potential sources be illuminated by the Sun may also be why the enhancements occur mostly in the region from 30°E to 120°E but rarely between 120° and 150°E and between 330° and 30°E. When MGS samples between 120° and 150°E, the source region resides in the east but still resides in shadow. As Mars rotates, MGS then samples from the region in the west (the region from 30°E to 120°E), and the potential sources move further toward the dayside and become illuminated. It is during that time that MGS records the enhancements. As Mars rotates further, the source region moves toward dusk on the dayside. Thus we do not observe enhancements between 330° and 30°E through 0°. Furthermore, Figure 9b shows the temporal distribution of the midlatitude of each enhancement (red dots) and the latitude of the source region (blue dots) at the time of the enhancement in the SS coordinate system. As the Martian season changes from spring to autumn the latitudes decrease. During spring, the source region remains at relatively high latitudes at the time it first sees the Sun each day. The source region's position moves to lower latitudes in the SS coordinate system as the Martian season changes from spring to autumn due to Mars' axial tilt. Thus Figure 9 implies that the enhancement location follows the crustal sources, strengthening their choice as the proposed origin of the low-energy electrons seen in the nightside enhancements.

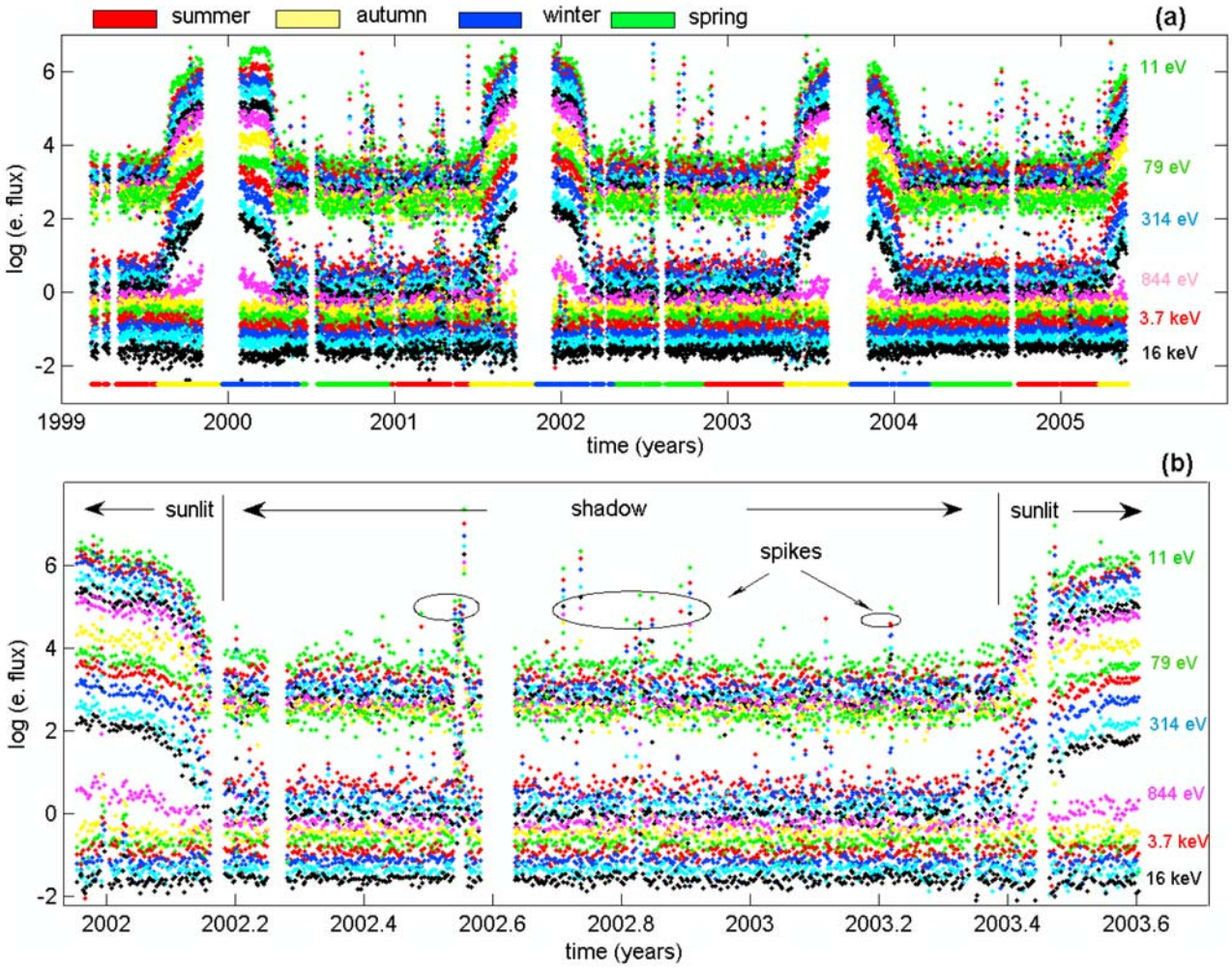

Figure 10. Temporal electron flux distribution over the closed crustal fields between 180° and 210°E and at ~65°S. (a) The logarithm of the omnidirectional electron fluxes at 19 energy levels (logarithmically spaced from 10 eV (top) to 20 keV (bottom) with an energy resolution of 25%). (b) Zoom of the electron flux during CY 2003. In Sun shadow, the electron flux drops to or below instrument background level revealing plasma voids (region marked under "shadow"). As the region is illuminated by the Sun, electron fluxes increase gradually filling the voids with photoelectrons (region marked under "sunlit"). "Spikes" seen in shadow are either due to the ambient electrons that can reach the voids such as aurora over nearby cusp regions or the disturbances driven by the transient solar ejections.

[22] It would be attractive to observe how the electron flux varies in the enhancement region during the day. But, the MGS orbit is fixed at 0200–1400 LT, and observing the daily variations in the electron flux distribution directly is not possible with MGS. However, over any given local geographical area, the temporal effect of the solar illumination may indeed be extracted from the MGS data. This is because the position of a local geographical point with respect to the Sun changes at the time MGS samples on the 0200–1400 LT meridian, due to precession of Mars' tilted rotation axis during the course of a Martian year. Such a sampled series of a special interest area can be mapped to a sequence. Thus we chose the local region between 180° and 210°E, and at around 65°S, where the crustal fields can exceed 200 nT at 400 km [*Connerney et al.*, 2001] and form closed fields and voids on the nightside [*Mitchell et al.*, 2001]. MGS orbits Mars about every 2 h and thus passes somewhere over this 30° wide crustal region once a day on the tailside of the terminator plane. The electron flux sequence obtained by this way, sampling the region once a day on the nightside over the 6 year time period, is plotted in Figure 10a (the 19 energy levels from top (10 eV) to bottom (20 keV) with an energy resolution of 25%; six of the energy levels are indicated next to corresponding curves on the right). During the northern late autumn and early winters, the region resides on the dayside of the terminator plane and thus the sequence has the gaps on the plot. In late spring and early summer, the region is in the deep dark at the time MGS takes samples, and thus the electron flux drops to the instrument background level due to loss via recombination and absorption [*Mitchell et al.*, 2001]. As the region moves from deep dark toward the edge of the

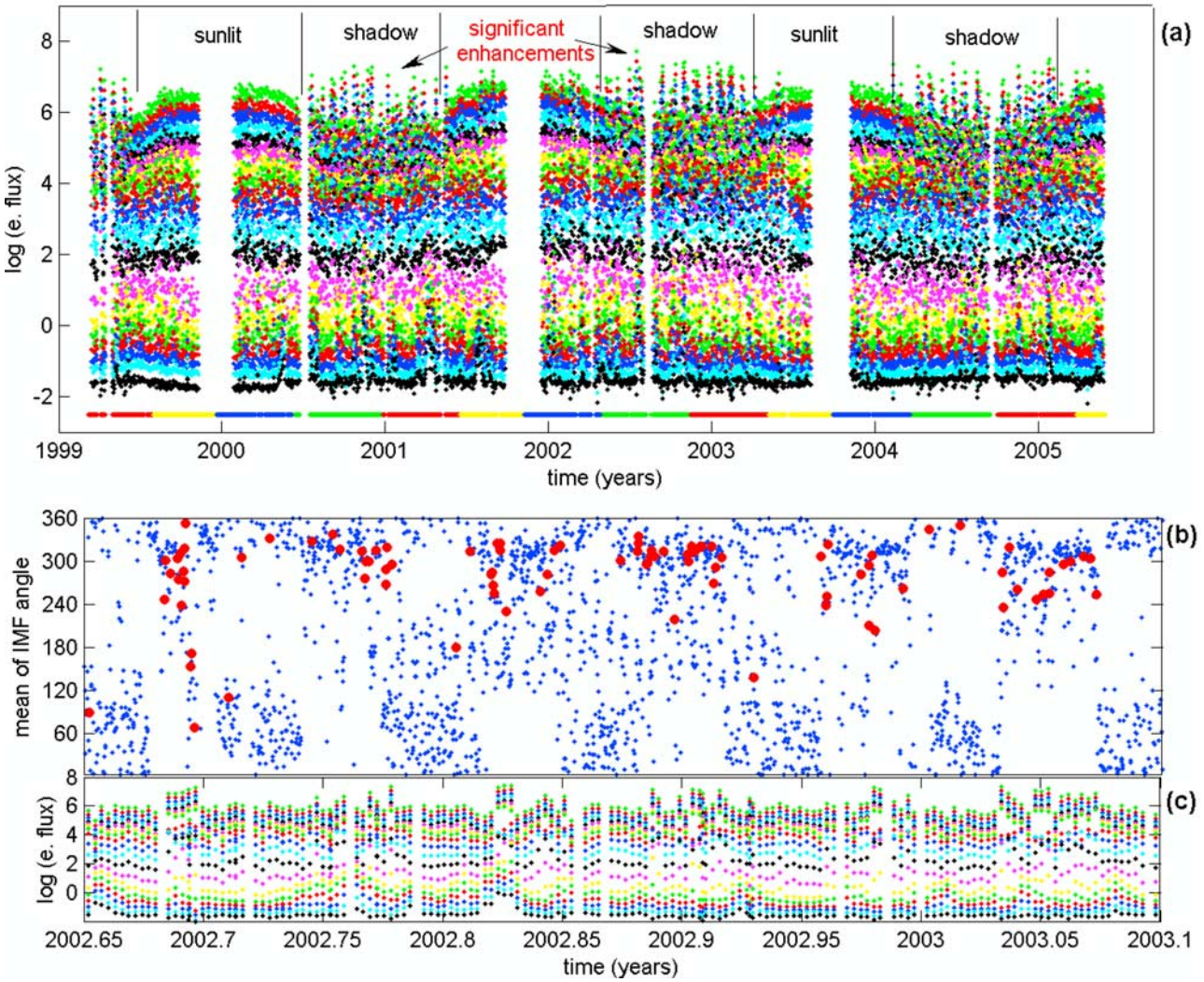

Figure 11. Temporal electron flux distribution over the geographical region for the significant enhancements (between 60° and 90°E, and at ~70°S.) (a) The logarithm of the omnidirectional electron fluxes at 19 energy levels (logarithmically spaced from 10 eV (top) to 20 keV (bottom), with an energy resolution of 25%). Spike-like outgrowths at the low energy levels are attributed to the significant enhancements. The enhancements are mostly observed in shadow, and there is a gradual increase in the typical nightside electron flux levels as the region starts to see the Sun (area marked as "sunlit"). (b) Expanded view of the estimated draped IMF angle during CY 2003 (from Figure 6a). The red dots mark the enhancements. (c) Expanded view of the electron flux during CY 2003. The enhancements are recognized by 2 orders of magnitude increase at the low energy levels and occur on a ~25 d periodic timescale coinciding with the westward alignment of the draped IMF.

terminator plane in late winter and early autumn, it starts to receive solar radiation at ~60°S, and the corresponding rise in the low-energy electron flux is apparent on the plot. The spike-like fluctuations in the nighttime may be either due to ambient electrons that can reach void regions, as explained in *Mitchell et al.* [2001], or to aurora seen in the neighborhood of the void [*Brain et al.*, 2006a]. These impulses in the intensity may also be driven by a sudden energy release or disturbance associated with solar flares or coronal mass ejections (CMEs) as they reach Mars or may even be caused by penetrating particles leading to anomalously high instrument background during certain periods such as passing CMEs.

[23] To observe the time evolution of the significant enhancements, we further investigated the enhancement region by using the same method described above. In section 3, we showed that the geographical area for the significant enhancements lies between 30° and 120°E, and at ~70°S. Furthermore, in this area most of the enhancements reside in a narrower band between 60° and 90°E (see Figure 2). To see the effect of the Sun striking this region, the electron fluxes (sampled on the tailside of the terminator plane once a day over the 6 year time period) are plotted in Figure 11a. In Figure 11a, each sample represents the average of the data that fall in the 5° wide latitude band around 70°S. During the northern late autumn and early

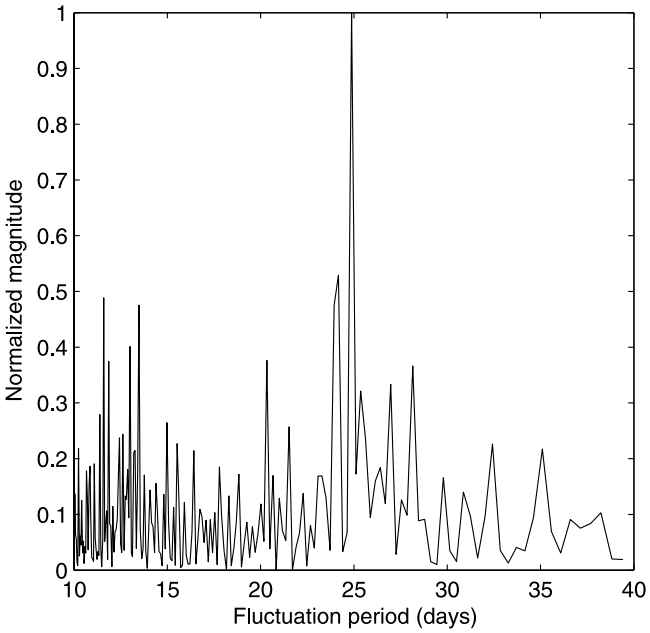

Figure 12. Normalized magnitude of the 116 eV omnidirectional electron flux as a function of fluctuation period. The 116 eV energy level lies almost near the geometric center of the energy band between 11 eV and a few hundred eV, over which the enhancements are observed. This energy band represents the general characteristics of the entire band.

winters, the region resides on the dayside of the terminator plane causing the gaps on the plot. A very interesting property of this plot is the emergence of the significant enhancement as spike-like outgrowths of the low-energy electron fluxes. Zoomed in view of the draped IMF direction (Figure 6a) at around CY 2003 is plotted in Figure 11b over the electron flux distribution plot in Figure 11c. A closer look at Figures 11b and 11c reveals that when the reconnection conditions are periodically met (Figure 11b, red dots), the low-energy flux enhancements occur periodically on an approximately 25 day timescale. (Note also that during some enhancements the highest energy channels, have elevated fluxes as well, which may be the result of passing transients in the solar wind such as CMEs, possibly penetrating particles artificially elevating the instrument count rate.) Figure 12 shows the normalized magnitude of the ~116 eV omnidirectional electron flux as a function of the fluctuation period obtained by FFT; the ~25 day periodicity is evident in this plot. The 116 eV energy level lies near the center of the energy band between 11 eV and a few hundred eV over which the enhancements are observed, representing roughly the general characteristics of the entire band. This evident correlation of the draped IMF direction with the enhancements suggests that the occurrence of enhancements is likely occur when the draped IMF has a westward direction than when the IMF is oriented elsewhere. Moreover, in Figure 11a, note the effect of solar illumination on the density of the electrons: as the season changes from early summer to late autumn, the region moves from deep dark toward the terminator plane and thus the electron flux level increases from the typical nightside value to typical dayside value. This increase corresponds to the time when this region reaches ~60°S in the SS coordinate system and is illuminated by the Sun. This effect is similar to that seen over the crustal fields mentioned previously but less pronounced. These two examples clearly present the general Sun radiation effect on the near Mars plasma while the first example explicitly shows the voids and the second example explicitly shows the enhancements observed on the nightside.

5. Magnetic Field Perturbations and Current Source Modeling

[24] As proposed in section 4, photoelectrons, produced over the crustal magnetic sources at ~150°E, ~65°S, follow the reconnected and draped field lines from the dayside to the nightside, contributing to the currents in the Martian magnetotail. The enhancements in the low-energy electron fluxes detected at the west side of the crustal sources may therefore be visible in the records of the MGS MAG instrument since the MGS orbit (see Figure 5) traverses these currents obliquely on the nightside. These currents would perturb the magnetic field distribution around them. We searched for these perturbations by comparing the MAG magnetic field measurements over the region between 30° and 120°E, and at ~70°S, when the enhancements are present with measurements taken at times when the enhancements are absent. A map obtained by averaging the magnetic field components in the absence of the enhancements shows that B_x, B_y and B_z remain below 8 nT, 4 nT and 3nT, respectively, over the enhancement region as expected because this region has no crustal sources [*Cain et al.*, 2003]. But, during an enhancement, the B_x and B_y components (in the SS coordinate system) can reach values of 15–25 nT and 5–10 nT, respectively. (The B_z component is still below 5 nT.) The nature of this behavior is shown in Figure 13. Note that the B_x and B_z components change sign from, $-B_x$ to $+B_x$, and $+B_z$ to $-B_z$, as MGS proceeds over the region where the enhancements occur. The overall magnetic field becomes almost zero at the time of the sign reversal, which coincides with the center of the enhancement region (Figure 1). Similar behavior in B_x in the induced lobe magnetic field due to current sheet crossings was noted by *Ferguson et al.* [2005] and *Halekas et al.* [2006]. These reversals in B_x and B_z imply a current flowing mainly in the azimuthal direction while the offset in the averaged B_y component implies a current flowing in the z direction. The estimated thickness of such a current is a few hundred kilometers along the latitudinal direction while its azimuthal extent can reach 2000 km. The perturbations in B_x can be explained by a current aligned in the azimuthal direction, with a surface current density of 0.1 $\mu A/m^2$.

[25] In this section, we model the currents that are responsible for the observed magnetic field perturbations. Our model begins with the approximation that the current sources are current dipoles placed in the vicinity of the enhancements. In this model, the dipole directions and their magnitudes are determined by least squares estimation process. To obtain these parameters, we devise a linear system of equations using the Biot-Savart law and the magnetic field measurements as follows.

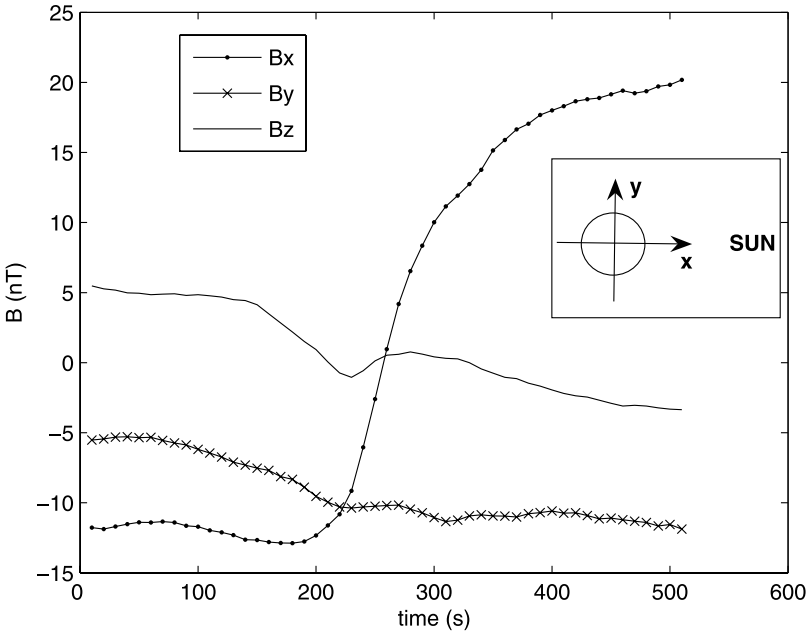

Figure 13. Averaged magnetic field components in the Sun-state coordinate system, obtained using the MAG data recorded at the times of enhancements.

[26] The magnetic field produced at r, by a current dipole at r′, with a moment Q is given by the Biot-Savart law:

$$\bar{B} = \left(\frac{\mu_0}{4\pi}\right)\frac{\bar{Q}(\bar{r}-\bar{r}')}{|\bar{r}-\bar{r}'|^3} \tag{2}$$

The total magnetic field measured at r is the sum of all the contributions from all of N current dipoles:

$$\bar{B}_{i\ total} = \sum_{n=1}^{N}\left(\frac{\mu_0}{4\pi}\right)\left(\frac{\bar{Q}_n(\bar{r}_i-\bar{r}_n')}{|\bar{r}_i-\bar{r}_n'|^3}\right) \tag{3}$$

At each MGS pass in which an enhancement is observed, we selected 50 magnetic field measurements in the vicinity of the enhancement along the MGS path such that the midpoint of the measurements coincides with the center of the enhancement. Then, the expression above is applied for each magnetic field measurement, $\bar{B}_i$, yielding an overdetermined linear system, **B** = **Ax**. In this system, **B** is a vector of M = 50 magnetic field measurements, i = 1 . . . 50, (3*M* samples since **B** is a vector), **A** represents the 3Mx3N matrix relating the current dipole moments to the field measurements, and x represents the 3N unknowns, $\bar{Q}_n$, (the intensity and direction of N current dipoles (vectors)) where M > N. The direct least squares solution of this system is nonunique and requires further constraint to impose the divergence free condition on the current (under static fields, $\nabla \cdot \mathbf{J} = 0$). Therefore the model was constrained by assuming that the dipoles located near the enhancement are aligned on a conduit-like shape. This approach led us to place a number of current dipoles at equal distances in a volume grid centered where B_x, the magnetic field component along the x axis in the SS coordinate system, is zero, i.e., the approximate center of the enhancement region. Both the distance between the dipoles, and the number of dipoles are test parameters. Our primary focus was finding the direction of these sources rather than their magnitudes. Furthermore, to satisfy the divergence-free current requirement and to obtain meaningful flow direction for the sources, we forced the current dipoles to be continuous by applying a regularization method:

$$F = ||Ax - B||^2 + \mu||Cx||^2 \tag{4}$$

In expression (4), **C** represents the matrix used in order to force the current continuity. The solution for **x** that minimizes **F** requires the matrix **A** to be full rank. This constraint limits the number of the current sources, which for our case is 30. The solution to our problem becomes

$$x = \left(A^T A + \mu C^T C\right)^{-1} A^T B \tag{5}$$

We estimated the directions of all dipoles, i.e., the flow direction of the possible current, that can generate the magnetic field perturbations associated with each enhancement. We found that almost every time an enhancement occurs, the current dipoles are directed toward the crustal magnetic source region, which is the proposed origin of the low-energy electrons flowing into the enhancement region: the electron flow should be opposite to current direction (i.e., away from the crustal sources). This result supports our interpretation of the significant enhancements observed on the nightside coming from the photoelectrons generated on the dayside above the crustal fields at 65°S and 150°E. Figure 14 illustrates the geometry, orbit, and current dipoles associated with a sample enhancement observed in the spring of 2000.

[27] In Figure 14, results are shown in the SS coordinate system. The green line shows the part of the orbit of MGS as it proceeds from north to south on the nightside. The

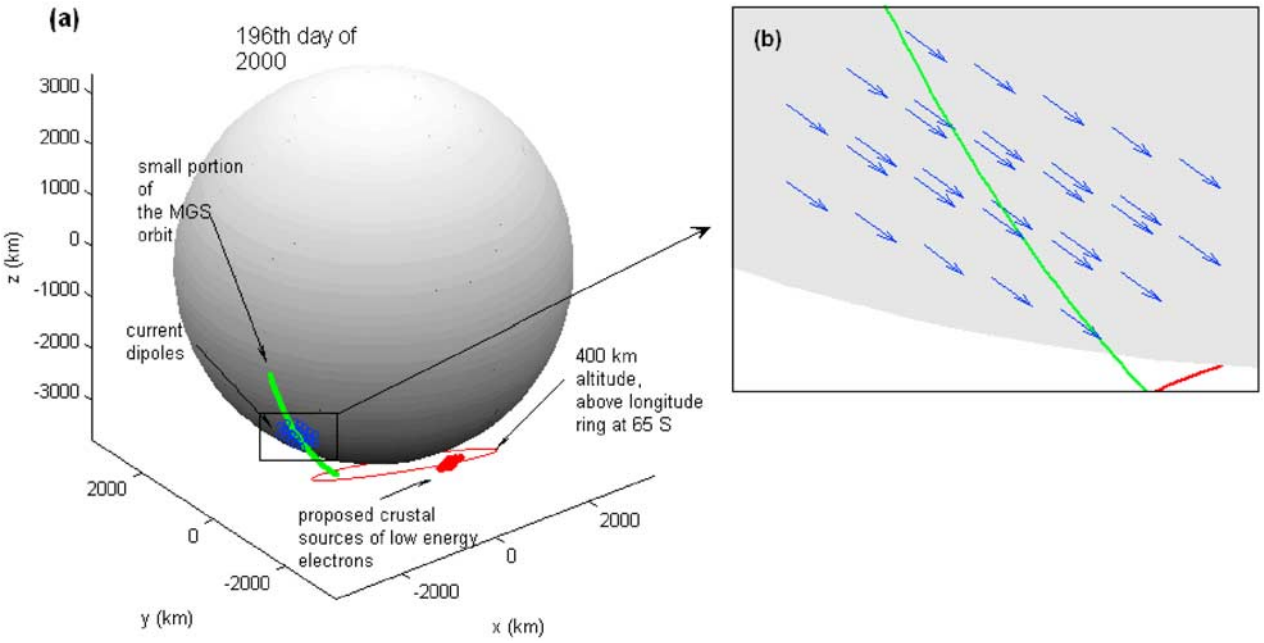

Figure 14. An example model of current sources at the time of an enhancement observed on the 196th day of 2000. (a) The view in the SS coordinate system. Current dipoles are displayed in blue and parameters were estimated using the MGS MAG data recorded along the portion of the orbit, marked in green. The red ring at the bottom is the 65°S parallel at an altitude of 400 km. The red rectangle on the ring represents the crustal magnetic fields at ∼150°E, 65°S, the region that is proposed as the origin of the low-energy electrons. (b) Zoom of the current dipoles of the model example on the 196th day of 2000.

same line also represents the magnetic field measurement positions used in the model. The red ring at the bottom is at the latitude of 65°S and an altitude of 400 km in the body-fixed coordinate system. The marked region (red rectangle) on the ring is the location of the proposed origin of the low-energy electrons (crustal sources at ∼150°E, 65°S). As illustrated, the marked crustal fields have an eastward alignment and see the Sun at the time an electron density enhancement is observed along the path of MGS marked in green. The estimated current source vectors (30 dipoles in this model) are shown in blue in the middle of the portion of the MGS path, and their zoomed view can be seen in Figure 14a. The distance between the current dipole sources was chosen to be 150 km. Note that the dipole sources point toward the crustal source and have a major component in the −y, a small component in +x, and a relatively small component in the ±z direction, as expected. We applied a similar method to each enhancement, and in each case the ensemble of current dipoles, as determined from the optimization discussed above, was remarkably similar in orientation and magnitude.

6. Conclusions

[28] In this study, our focus was on significant enhancements observed in the MGS omnidirectional electron flux data that occur at low-energy levels (below a few hundred eV), clustered over a geographical region located between 30° and 150°E, and at ∼70°S, and occur favorably in the northern hemisphere's late spring and early summer, with a ∼25 day periodicity.

[29] The low-energy nature of the enhancements suggests that the source of the particles is the photoelectrons generated on the dayside over the crustal magnetic fields, which are located near ∼150°E and ∼65°S. The closed magnetic field lines over the crustal field region are oriented eastward, and most of the enhancements occur when the draped IMF is directed westward, supporting the notion of reconnection of fields during the observation of these events. Thus we propose that the reconnected and draped field lines carry the low-energy ionospheric electrons from the dayside to the nightside and form a current in the tail. The conditions for reconnection occur much more frequently in the late spring and early summer. The short-term periodicity, on a ∼25 day scale, seen in both the draped IMF direction and the occurrence times of the enhancements further supports the role of the IMF and its orientation.

[30] We have proposed a model for the distribution of current sources that can generate the perturbations detected in the magnetic field data in the vicinity of the enhancements. In this model, candidate current sources are represented by current dipoles located in proximity to the enhancements, and their directions are determined by utilizing the MGS MAG data measurements in a consistent optimization. An optimum solution for the dipole ensemble is obtained by the application of the least squares and regularization methods which satisfy a current continuity condition. It is seen that the least squares estimated current dipoles are always aligned toward the crustal sources that are the proposed origin of the low-energy electrons. This is consistent with and supports the hypothesis that photoelectrons generated over the magnetic crustal source regions

on the dayside are the source of the enhancements detected by MGS on the nightside of Mars. The photoelectrons follow the field lines from the dayside to the nightside and form currents in the tail.

[31] **Acknowledgments.** This work was supported by the grant from the Bosack-Kruger Foundation. We acknowledge valuable discussions with Martin Walt and Husrev Tolga Ilhan. We also thank the Planetary Data System for providing the data used in this work.

References

Acuña, M. H., et al. (1992), Mars Observer magnetic fields investigation, *J. Geophys. Res.*, *97*(E5), 7799–7814.

Acuña, M. H., et al. (1998), Magnetic field and plasma observations at Mars: Initial results of Mars Global Surveyor mission, *Science*, *279*, 1676–1680.

Acuña, M. H., et al. (1999), Global distribution of crustal magnetization discovered by the Mars Global Surveyor MAG/ER experiment, *Science*, *284*, 790–793.

Acuña, M. H., et al. (2001), Magnetic field of Mars: Summary of results from the aerobraking and mapping orbits, *J. Geophys. Res.*, *106*(E10), 23,403–23,417.

Brain, D. A., F. Bagenal, M. H. Acuña, and J. E. P. Connerney (2003), Martian magnetic morphology: Contributions from the solar wind and crust, *J. Geophys. Res.*, *108*(A12), 1424, doi:10.1029/2002JA009482.

Brain, D. A., J. S. Halekas, L. M. Peticolas, R. P. Lin, J. G. Luhmann, D. L. Mitchell, G. T. Delory, S. W. Bougher, M. H. Acua, and H. Rme (2006a), On the origin of aurorae on Mars, *Geophys. Res. Lett.*, *33*, L01201, doi:10.1029/2005GL024782.

Brain, D. A., D. L. Mitchell, and J. S. Halekas (2006b), The magnetic field draping direction at Mars from April 1999 through August 2004, *Icarus*, *182*(2), 464–473.

Cain, J. C., B. B. Ferguson, and D. Mozzoni (2003), An $n = 90$ internal potential function of the Martian crustal magnetic field, *J. Geophys. Res.*, *108*(E2), 5008, doi:10.1029/2000JE001487.

Connerney, J. E. P., M. H. Acuña, P. J. Wasilewski, N. F. Ness, H. R'eme, C. Mazelle, D. Vignes, R. P. Lin, D. L. Mitchell, and P. Cloutier (1999), Magnetic lineations in the ancient crust of Mars, *Science*, *284*, 794–798.

Connerney, J. E. P., M. H. Acuña, P. J. Wasilewski, G. Kletetschka, N. F. Ness, H. R'eme, R. P. Lin, and D. L. Mitchell (2001), The global magnetic field of Mars and implications for crustal evolution, *Geophys. Res. Lett.*, *28*(21), 4015–4018.

Crider, D. H. (2004), The influence of crustal magnetism on the solar wind interaction with Mars: Recent observations, *Adv. Space Res.*, *33*, 152–160.

Dubinin, E., et al. (2006a), Solar wind plasma protrusion into the martian magnetosphere: ASPERA-3 observations, *Icarus*, *182*, 343–349.

Dubinin, E., et al. (2006b), Electric fields within the martian magnetosphere and ion extraction: ASPERA-3 observations, *Icarus*, *182*, 337–342.

Dubinin, E., et al. (2006c), Plasma morphology at Mars. ASPERA-3 observations, *Space Sci. Rev.*, *126*, 209–238.

Fedorov, A., et al. (2006), Structure of the Martina wake, *Icarus*, *182*, 329–336.

Ferguson, B. B., J. C. Cain, D. H. Crider, D. A. Brain, and E. M. Harnett (2005), External fields on the nightside of Mars at Mars Global Surveyor mapping altitudes, *Geophys. Res. Lett.*, *32*, L16105, doi:10.1029/2004GL021964.

Frahm, R. A., et al. (2006a), Carbon dioxide photoelectron energy peaks at Mars, *Icarus*, *182*, 371–382.

Frahm, R. A., et al. (2006b), Locations of atmospheric photoelectron energy peaks within the Mars environment, *Space Sci. Rev.*, *126*, 389–402.

Halekas, J. S., D. A. Brain, R. J. Lillis, M. O. Fillingim, D. L. Mitchell, and R. P. Lin (2006), Current sheets at low altitudes in the Martian magnetotail, *Geophys. Res. Lett.*, *33*, L13101, doi:10.1029/2006GL026229.

Krymskii, A. M., T. K. Breus, N. F. Ness, M. H. Acuña, J. E. P. Connerney, D. H. Crider, D. L. Mitchell, and S. J. Bauer (2002), Structure of the magnetic field fluxes connected with crustal magnetization and topside ionosphere at Mars, *J. Geophys. Res.*, *107*(A9), 1245, doi:10.1029/2001JA000239.

Mitchell, D. L., R. P. Pin, C. Mazelle, H. R'eme, P. A. Cloutier, J. E. P. Connerney, M. H. Acuña, and N. F. Ness (2001), Probing Mars' crustal magnetic field and ionosphere with the MGS Electron Reflectometer, *J. Geophys. Res.*, *106*(E10), 23,419–23,427.

Nagy, A. F., D. Winterhalter, and K. Sauer (2004), Plasma environment of Mars, *Space Sci. Rev.*, *111*, 33–114.

Ness, N. F., M. H. Acuña, J. E. P. Connerney, A. J. Kliore, T. K. Breus, A. M. Krymskii, P. Cloutier, and S. J. Bauer (2000), Effects of magnetic anomalies discovered at Mars on the structure of the Martian ionosphere and solar wind interaction as follows from radio occultation experiments, *J. Geophys. Res.*, *105*(A7), 15,991–16,004.

Purucker, M., D. Ravat, H. Frey, C. Voorhies, T. Sabaka, and M. Acuña (2000), An altitude normalized magnetic map of Mars and its interpretation, *Geophys. Res. Lett.*, *27*(16), 2449–2452.

Soobiah, Y., et al. (2006), Observations of magnetic anomaly signatures in Mars Express ASPERA-3 ELS data, *Icarus*, *182*, 396–405.

I. Linscott and D. Uluşen, Department of Electrical Engineering, 161 Packard Building, 350 Serra Mall, Stanford University, Stanford, CA 94305-9505, USA. (dulusen@stanford.edu)